Title
Joule Heated Reactor Design for Methane Conversion

Author
Ke, Jun

Publication Date
2021

Peer reviewed|Thesis/dissertation

UNIVERSITY OF CALIFORNIA

Los Angeles

Joule Heated Reactor Design for Methane Conversion

A thesis submitted in partial satisfaction

of the requirements for the degree of Master of Science

in Chemical Engineering

by

Jun Ke

2021

ABSRACT OF THE THESIS

Joule Heating Reactor Design for Methane Conversion

by

Jun Ke

Master of Science in Chemical Engineering

University of California, Los Angeles, 2021

Professor Panagiotis D Christofides, Chair

As the global energy demand continues to increase, there is a growing focus on the use of renewable electricity as a source of energy to power the transportation, industrial, manufacturing, and commercial/residential sectors of our economy. Although the cost of renewable electricity from wind and solar is decreasing, the world still lacks large scale energy storage technologies that could allow us to use renewable energy even at night or when there is no wind. Fossil fuels are

solar energy that was stored millions of years ago. However, fossil fuels are not only the main sources of energy for the residential/commercial and transportation sectors but these are also sources of carbon and hydrogen feedstocks for industrial manufacturing which makes it difficult to abate carbon emissions from these sectors. There is a need to develop sustainable energy generation systems that either replace fossil fuels entirely or that when combined with the use of fossil fuels, diminish the overall greenhouse gas emissions and pave the way for the utilization of clean energy in the future in a manner that is sustainable.

This thesis describes research on the use of Joule heating of a FeCr alloy tube washcoated with a Ni/ZrO_2 catalysts. Two types of reactions are tested over this catalyst, CO_2 methanation and steam methane reforming (SMR). Herein, we describe a systematic study of the catalyst activity, the dependance of performance in temperature, and a description of the temperature profiles generated over the alloy tube during testing. This work describes synthetic routes for the deposition of catalytic washcoats and how deposition parameters affect reactor performance. The results generated in this work, demonstrate that indeed the electrification of traditional chemical reactors is possible and establish a new research capability in the Morales-Guio group.

Applying Joule heating to tube reactors provides several benefits compared to radiant and convective heat transfer in industrial reformer furnaces. This thesis work describes the optimization of the washcoating procedure and how these are related to performance. The delivery of heat through Joule heating increases the rate at which energy is provided to the catalysts and influences performance. The catalyst washcoat deposition method influences the active metal mass loading and the washcoat morphology which affects mass transport to the catalytic sites inside the tube surface. Joule heating eliminates thermal gradients between the heat source and the catalysts

by decreasing the distance between heat generation and heat consumption on the catalysts. Moreover, it reduces waste gases associated with fuel combustion in furnaces. Finally, the electrified reactor is compact, efficient and amenable to scaling up granted benchmarks of activity and stability are met.

Experimental results suggest that there is a difference between external heating and Joule heating of a reactor even when the reactor tube temperature is the same. For both reactions studied in this work, Joule heating methods provide better catalyst performance. Under CO_2 Methanation reaction, Joule heating generates a higher methane production rate and also leads to the formation of ethane. For SMR, the activity of the catalyst decreases and could be caused by coke formation. The deactivation mechanism is not well understood in this system and further experiments are required.

In summary, Joule heating is a viable approach for the supply of heat in industrially relevant reactions such as SMR and other endothermic processes. The reduced flue gas generation associated with the electrification of furnaces, reduced reactor volume and improvements in catalysts efficiency could provide a unique opportunity for the electrification of industrial chemical production processes. Electrification of chemical manufacturing processes could result in cleaner and more efficient production plants compared to existing chemical manufacturing lines. Electrification of chemical production is an important step towards the decarbonization of the industrial sector and the development of sustainable chemical manufacturing units.

The thesis of Jun Ke is approved.

Carlos G. Morales-Guio

Dante A Simonetti

Panagiotis D Christofides, Committee Chair

University of California, Los Angeles

2021

Table of Contents

ABSRACT OF THE THESIS ii

List of Figure viii

List of Tables x

Acknowledgements xi

1. Introduction 1

2. Background 2

2.1 Joule heating 2

2.2 Washcoating 4

2.3 CO_2 methanation 6

2.4 Steam methane reforming 8

3. Experimental Setups 9

3.1 Reactor Setup 9

3.2 Catalysts Preparation 10

3.3 Analysis of reactant and product Gases 11

3.4 Description of the testing system 12

4. Results and Discussion 13

4.1 Joule heating 13

4.2 Optimization of washcoating to stainless steel tubes 16

4.3 Catalysts Characterization 19

4.4 CO_2 Methanation with various coated stainless-steel tubes 19

4.5 Comparison between external heating and Joule heating 24

4.6 Steam Methane Reforming 27

5. Conclusion and Outlook 30

Appendices 32

Appendix. A GC calibration 32

Appendix. B Activation Energy 34

Appendix. C Supplementary Figures and table 36

References 38

List of Figure

Figure 2.3. 1. Simplified mechanism of CO_2 methanation. 7

Figure 3.1. 1. An assembly of Joule heated tube reactor 10

Figure 3.4. 1. Entire reaction set-up including gas inlets, reactor, power supply, condenser and GC in the Simonetti lab. 13

Figure 4.1. 1. Joule heated tube reactor with multiple testing position (P1: midpoint, P2 and P3: outer points) for thermal measurements. 14

Figure 4.1. 2. Temperature vs. current curves for initial heating test on a Joule heated tube, blue points are temperature measured without insulation, orange points are temperature measured with insulation. 14

Figure 4.1. 3. Temperature vs current curves for initial heating test on a Joule heated tube, T1 is temperature measured on a Joule heated reactor in fume hood, T2 is temperature measured on a Joule heated reactor in furnace test system (Figure.3.4.1). 15

Figure 4.2. 1. ZrO_2 loading changing with tube length and number of coatings. 1 corresponds to one time coating and 2 and 3 corresponds to the repetition of the coating procedure two and three times, respectively. 16

Figure 4.2. 2. Overall thickness of zirconia layer in steel tube. (The thicknesses are calculated based on the zirconia weight, assuming a porosity and finding what the theoretical thickness would be if evenly coated over the entire tube inner surface.) 1, 2, and 3 indicates the overall thickness of zirconia with one-, two-, and three-time coatings, respectively. 17

Figure 4.2. 3. ZrO_2 loading vs slurry concentration 18

Figure 4.3. 1. Comparison of SEM images of Ni/ZrO_2 catalysts removed from stainless steel tube (A) and FeCr alloy tube (B) 19

Figure 4.4. 1. Production rates of CH_4 (A) and CO (B) vs. temperature for comparison between stainless steel tube 1 and 2. 21

Figure 4.4. 2. CH_4 (A) and CO (B) production rate vs. temperature for comparision of various stainless steel tubes. (Tube # 2,3,3R, and 4, related preparing information in Table 1)..... 22

Figure 4.4. 3. CH_4 selectivity (A) and nomarlized production rate (B) vs. temperature on various stainless steel tubes with different thicknesses of washcoat. 23

Figure 4.5. 1. Normalized methane production rate vs. temperature for comparing FeCr alloy tube (7) with various stainless steel tubes (2, 3R, 6) with different thickness of washcoat. 24

Figure.4.6 1. CH_4 Conversion (A) and H_2 production (B) vs. temperature for comparison between stainless tube 6 and FeCr alloy tube 7 27

Figure.4.6 2. CH_4 conversion vs temperature for FeCr alloy tube 7 at fixed current. 29

Figure.4.6 3. CH_4 conversion for FeCr alloy tube 7 observed at 750 ℃ and 850 ℃ with varying current. 29

Figure A. 1. GC calibration curve for H_2. 32

Figure A. 2. GC calibration curve for CO_2. 33

Figure A. 3. GC calibration curve for CH_4. 33

Figure B. 1. The Arrhenius plot of ln r as a function of 1/T, the calculated activation energy shown in Table 2, (A) is Tube 6 (Ni/ZrO_2(x2)/SS/5), (B) is Tube 7 (Ni/ZrO_2(x2)/FeCr/5), (C) is Tube 3R(Ni/ZrO_2(x4)/SS/5). 35

Figure C. 1. The initial heating set-up with labeled thermocouples. 36

Figure C. 2. The prepared 15% ZrO_2 slurry (A) and 0.1 M nickel nitrate solution (B). 37

Figure C. 3. The nickel catalysts are well coated to steel tube, the light green powder contains zirconia and nickel. 37

List of Tables

Table 1. Multiple tubes were prepared by different parameters including number of coatings, tube materials, catalysts loading, removed end catalysts, heating method and nomenclature in this study. 20

Table 2. Calculated activation energy for tube 6 (Ni/ZrO_2(x2)/SS/5), 7 (Ni/ZrO_2(x2)/FeCr/5) and 3R(Ni/ZrO_2(x4)/SS/5). 26

Table 3. The measured temperature profile of experiment shown in Figure C.1. 36

Acknowledgements

First of all, I would sincerely like to thank my supervisors Prof. Carlos Morales Guio for his guidance and support. With his instruction and comments, I can finish my project very well. I would also like to thank Prof. Dante A Simonetti for his exceptional advice and support in his lab.

It was truly a pleasure to work with my colleague, Derek Richard. For his help, and discussion, I learn a lot from him. Also, I would like to thank Eric Lin for his guidance on experimental instruments. Further, I would like to thank all other group members to create a friendly and wonderful environment.

Finally, I would like to thank my family and friends who always support me to pursue my goals. Without them, I cannot insist to my study in the United State.

1. Introduction

Methane is a strong greenhouse gas contributing significantly to global warming due to its significant absorption in the infrared spectrum. Methane absorbs, per molecule, more thermal infrared radiation than CO_2 and has over 30 times higher global warming potential.[1] The mole fraction of methane in the atmosphere reached 1857 ppb in 2018, which is 2.6 times higher than in 1750.[2] The increase in methane in the atmosphere is mainly due to the growing utilization of fossil fuels, the increase in methane emissions from cattle and agricultural applications, and emissions from municipal waste.[1,3] Methane not only contributes to global warming, but also increases tropospheric ozone levels.[3] Although methane emissions are harmful to the environment, methane and natural gas are the best option available towards transitioning away from other fossil fuels such as coal and petroleum. This is because methane produces less CO_2 emissions and pollutants per unit of energy delivered compared to all other fossil fuels. Methane is broadly used for the production of chemicals and is the preferred source of energy in the industrial sector. In order to reduce greenhouse gas emissions associated with natural gas exploitation and utilization, many research efforts have been dedicated to the development of catalytic methane conversion systems for the direct transformation of methane into chemicals and fertilizers with reduced greenhouse gas emissions.

Due to the limited reserves of fossil fuels and the effects that their use has on global warming, the replacement of fossil sources of energy by renewable ones has attracted people's imagination.[4] Renewable sources of energy are being called to play an essential role in the future. However, it is not easy to replace fossil fuels. Most sources of renewable energy are produced by water, wind, solar, and others which are of an intermittent nature and require large scale energy storage mechanism.[4,5] Electrochemistry is a viable alternative to transform renewable electricity

into chemical energy and make essential base chemicals that are used in the production of everyday goods. Converting power to hydrogen is a good alternative to store energy, however, the cost for electrochemical hydrogen generation from water is still very high.[6–8]

Currently, SMR converts methane to hydrogen for use in a wide range of essential chemical processes, including methanol, and ammonia synthesis. SMR requires harsh conditions (high temperature and pressures) to reach economic production rates and requires complex heat integration systems to achieve high system energy efficiency. Recent literature has shown the conversion of methane to hydrogen via electrical heating utilizing Joule heated reactors.[9] This method of heating could provide an alternative to the conventional method of using gas fired heaters to provide heat to endothermic processes. In this thesis, Ni/ZrO_2 catalyst has been utilized in a Joule heated reactor to investigate CO_2 hydrogenation and SMR. The study aims to optimize a lab scale Joule-heated reactor and better understand the preparation method of a washcoated catalyst. This reactor heating method combined with washcoated catalysts provides a new configuration of reactor design for SMR and CO_2 methanation.

2. Background

2.1 Joule heating

Joule heating is induced by passing an electric current through a conductor. The heat generation is mainly due to the resistance of the conductor which depends on the material and geometry. Heat flux and temperature is controlled by the power supply and electrical resistance (R) of the metal. The heat flux is related to the power by equation 2.1.1, where P is power, I is current, V is voltage and R is resistance.[10] According to the above equation, a higher material

$$Heat = P = I^2R = V^2/R \quad (2.1.1)$$

resistance will lead to a higher heat flux for the same applied current resulting in a higher temperature of the working surface. Thus, to enable easy temperature control, it is desired to use metals with temperature-independent resistance.[11]

Joule heating provides many advantages over gas traditional fired heaters. First, it possesses rapid temperature response corresponding to current changes.[10,11] Ideally, once the current is adjusted to a new value, the temperature should change quickly. Second, Joule heating applied in thermochemical system creates cleaner working environments due to elimination of fuel combustion processes. Third, this direct heating of the reactor wall eliminates axial temperature gradients often observed in the metal tube that can cause additional stresses on the reactor body in fired heaters.[12] Lastly, Joule heating allows the delivery of large duties within smaller configurations which means more compact, economical, and efficient thermal manufacturing units. to the target catalyst.

Utilization of Joule heating for endothermic chemical reactions is well documented in literature.[15] In one of these processes, a heated rod was inserted into the packed bed as a heat source for pyrolysis of hydrocarbons.[13] In a second system, a conductor coated with a catalyst was used to demonstrate dry methane reforming. In the experiment, heating elements consisting of a FeCr alloy were coated with a $LaNi_{0.95}Ru_{0.05}O_3$ catalyst.[14] Additionally, Kameyam et al. has shown that implementation of anodized FeCrNi Alloy could provide improved electrically heated SMR reactors with a short start up time and long-term stability.[15]

Recently Sebastian et al. compared a washcoated Joule heated reactor to conventional SMR demonstrating how this configuration of a Joule heating reactor could offer advantages over conventional processes.[13] This approach utilizes the intimate contact between heat source and the

catalysts in the washcoat to remove thermal limitations and provide improved control of the SMR reaction. In addition, it was shown how conversion of existing SMR operations to Joule heated systems could reduce the global CO_2 emission by 1%. Not only did this method of SMR offer better operation conditions, such as a lower steam/methane ratio, but it also provided a higher methane conversion rate. Overall, Joule heated reactors could provide the advantages of reduced capital cost, increased operation control, and environmentally friendly SMR processes.

2.2 Washcoating

Typically, conventional SMR is conducted in a pack-bed reactor in the presence of heterogenous catalysts. Due to axial thermal gradients caused by the endothermicity of SMR, much of this catalyst bed is underutilized. In comparison, reactor coils prepared by washcoating methods only place catalyst near the wall of the reactor tube.[18] By applying Joule heating to the reactor wall, heat is evenly transferred to the catalyst, maximizing its effectiveness.

FeCrAl Alloy can be used as the heating support for heterogeneous catalysts. Under reaction condition of high temperature and pressure, the aluminum oxide component in the alloy protects the other metals from oxidation.[16–18] Normally, the oxide layer forms over the surface of the metal and prevents reactants from interacting with iron or chromium in the alloy. This is especially important for iron since significant oxidation of this component could affect the structure and physical properties of the alloy. The presence of an oxide layer on the surface of the metal alloy also promotes the formation of bonds between the metal oxide layer and the metal oxide used as catalyst support in washcoats, increasing the adhesion of the washcoat to the tube surface.[19]

Multiple methods can be used to deposit the washcoat on the alloy surface, such as colloidal coating, sol-gel, and slurry coating.[19] Adhesion of the metal oxide catalyst support is controlled by the viscosity of the slurry and the drying procedure.[20,21] Commonly, the stability of the slurry is adjusted by the electrostatic environment.[22] This means, matching the zeta potential of the particles with that of the substrate to favor adhesive electrostatic interactions. Generally, metal materials will have better dispersion under an acidic environment.[23,24] The type of acid selected for these processes can depend on the catalyst preparation method, but normally nitric acid is used to adjust the pH. Higher zeta potential represents higher electrostatic repulsion between particles in the same medium. Zirconia, for example, has maximum zeta potential at a pH of 4. This pH adjusting method allows the surface of metal oxide particles to have positive charge and promotes uniform adhesion between the metal surface and oxide support. In addition, some organic binders are often used to enhance washcoat adhesion, but this method will not be discussed in detail here. The pH, the binder and other factors must be optimized to have a stable and low viscosity slurry to improve coating adhesion and uniformity.[25]

In addition to slurry application, several other preparation steps, such as drying, calcination, and pretreatment play important roles in the washcoating performance. First, the drying parameters, such as temperature, time, and other factors, may have some effects on mass loading and coating uniformity.[26] For example, high drying temperature decreases the Brunauer-Emmett-Teller (BET) surface area of washcoated catalysts and enhances the crack formation over the catalysts surface. The cracks would result in weight loss during catalytic site deposition process. Secondly, the duration and temperature of the washcoat calcination step may affect particle sizes and structure. Finally, chemical, or thermal pretreatment on metal support is an optional choice to have a better coating adhesion by adjusting physical properties of the metal surface.[27–29] The pretreatment will

increase the roughness of the metal surface and improve coating adhesion. This adjustment will ameliorate the catalytic durability on the reactor wall while still maintaining certain amount of mass loading.

Lastly, wet impregnation is a common technique for adding catalyst active sites to metal oxide supports. Typically, the advantages of this method are the simple impregnation process, cost effectiveness, and minimal amount of waste.[32] The loading of active sites is controlled by the concentration of precursor solution; Therefore, higher mass loading can be achieved by using precursors with higher concentration during the catalyst deposition. As an example, metal nitrates are typically selected as a precursor to prepare nickel oxide catalysts.

2.3 CO_2 methanation

CO_2 methanation is a useful reaction for the conversion of greenhouse gases into a usable resource, methane. This is an exothermic reaction typically carried out at temperatures lower than 500℃. To date, catalysts mechanistic investigations have provided inconsistent results and there is still no consensus regarding the reaction mechanisms governing this transformation.[30] The two possible pathways considered to produce methane are: 1) a mechanism where CO_2 is converted into CO as the intermediate, then CH_4 is derived from either hydronated CO (-HCO-) or C atom (-C-), and 2) a direct CO_2 methanation mechanism where the bicarbonate (-HCO_3) or other species (-HCOO-) are the reaction intermediate.[31] (Figure 2.3.1).

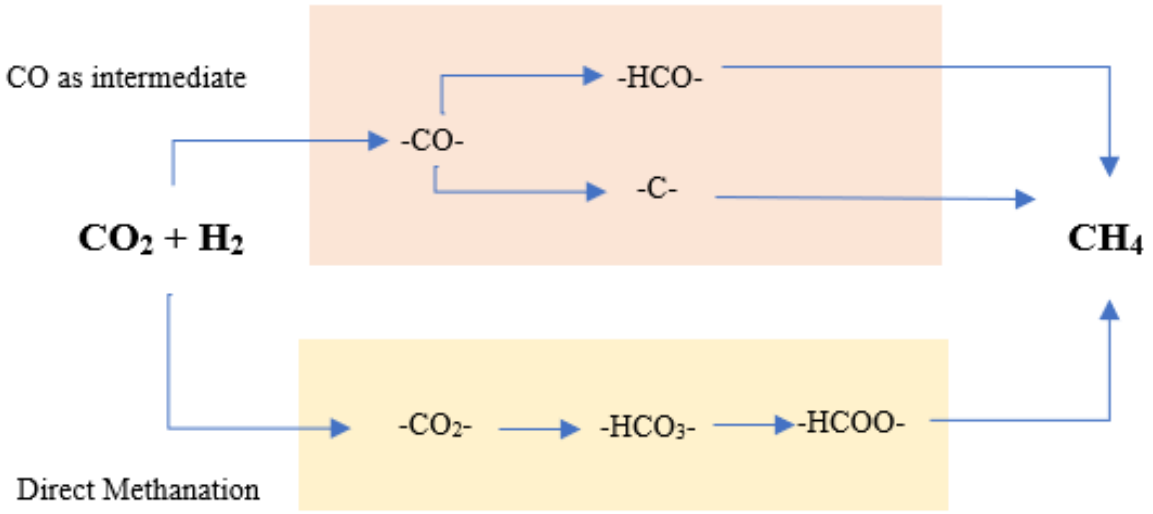

Figure 2.3. 1. Simplified mechanism of CO_2 methanation.

Transition metals (e.g., iron, cobalt, copper, nickel) have been shown to be active catalysts for CO_2 methanation.[18] Adsorption of carbon dioxide on transition metals is thermodynamically favorable, and the surface microstructure of the metal strongly affects the energetic barrier for CO_2 activation and reduction steps during the catalytic process.[32] Ni is of interest as a catalyst for CO_2 methanation due to its low cost and high efficiency for this reaction. Several different support materials have been investigated to enhance nickel's catalytic activity, such as alumina, zeolites, SiO_2, CeO_2, ZrO_2, carbon nanotubes, and other unconventional supports.[31–33] The metal oxide supports not only change the catalyst dispersion, but also affect the intrinsic activity through metal-support interactions. As such supports are commonly used to improve the catalyst performance.

In this study, a nickel catalyst supported on a zirconia washcoat is fabricated and tested for CO_2 methanation. Zirconia is chosen as the support because of its strong CO_2 adsorption which could help enhance CO_2 methanation by shifting the thermodynamic equilibrium at the catalyst surface by hydrogenation of CO_2. The strong CO_2 adsorption maintains higher local concentration

of CO_2 than bulk. The reaction rate of CO_2 methanation would be slower than the adsorption rate so that the catalyst surface has a net accumulation of CO_2 adsorption. Moreover, monoclinic- ZrO_2 displays high thermal stability at high temperatures.

2.4 Steam methane reforming

Steam methane reforming is currently the primary method of producing hydrogen.[37] Since hydrogen is likely to be used as a clean energy vector in the future, recent efforts have been devoted to developing greener steam methane reforming technologies in order to produce hydrogen in a manner that is cost effective and environmentally friendly.[34]

In the steam methane reforming reaction, the following reactions produce a mixture of hydrogen, carbon dioxide, and carbon monoxide called syngas.[8,35]

$$CH_4 + H_2O \leftrightarrow CO + 3H_2 \quad \Delta H^o_{298\,K} = 206.4\ kJ/mol \tag{2.4-1}$$

$$CO + H_2O \leftrightarrow CO_2 + H_2 \quad \Delta H^o_{298\,K} = -41.2\ kJ/mol \tag{2.4-2}$$

$$CH_4 + CO_2 \rightarrow 2CO + 2H_2 \quad \Delta H^o_{298\,K} = 247.3\ kJ/mol \tag{2.4-3}$$

Equation (2.4-1) is the methane reforming reaction. Equation (2.4-2) shows the water gas shift reaction and equation (2.4-3) shows CO_2 reforming or dry reforming. The overall process is a highly endothermic reaction. Additionally, methane is a highly symmetrical and non-polar molecule that is difficult to activate. Therefore, this reaction requires a large amount of energy to activate methane and balance the endothermicity of the reaction. Normally, the process is implemented under conditions of high temperatures and pressures with nickel-based catalysts to provide industrially relevant production rates.

$$CH_4 \rightarrow C + 2H_2 \quad \Delta H^o_{298\,K} = 74.9\ kJ/mol \tag{2.4-4}$$

$$2CO \rightarrow C + CO_2 \quad \Delta H^o_{298\,K} = -172.5\ kJ/mol \tag{2.4-5}$$

At high temperature, the coke formation would happen over catalyst surface, and it is related to methane decomposition (equation 2.4-4) and the Boudouard reaction (equation 2.4-5). Both reactions produce carbon that can deposit on the catalytic surface, block the active site, inhibit the SMR process and affect the mechanical stability of the catalyst.[8,35] In order to reduce coke formation, some works in literature have shown a new type of Ni-based catalysts doping with traces of sulphur or metals[35,36], that show promising catalyst application for SMR in the future. The cokes formation is influenced by factors such as the catalyst particle size, shape, structure, and composition. Particularly, particle size is the most significant factor. If the Ni particle size could reach the magnitude of nanometers, then, it would perform neglectable effects of coke formation during methane reforming reaction.[35,37,38] However, synthesis and preparation of such small size particle catalysts remain challenging.

3. **Experimental Setups**

3.1 Reactor Setup

In a typical reactor (Figure 3.1.1), the one-quarter-inch fittings (supplied by Swagelok) are connected to both ends of the FeCr alloy tube (supplied by Goodfellow) with 500 mm length and 6 mm outer diameter. A copper plate is cut and bent into two copper sockets which are attached on both sides of tube. The assembly of the copper sockets and the tube is shown in the Figure 3.1.1. The sockets with stainless steel bolts are used to connect electrical wires from the power sources. 1 AWG welding grade cables are used as both positive and negative leads to provide current from the power supply. The Ni/ZrO_2 washcoated catalyst is applied to the internal surface of the tube

by slurry coating and wet impregnation. During the catalyst testing, the whole tube is covered by insulation to prevent heat loss.

Figure 3.1. 1. An assembly of Joule heated tube reactor

3.2 Catalysts Preparation

To apply the catalytic washcoat to the reactor tube, zirconium (IV) oxide (powder, 5μm, 99% trace metals basis), nickel (II) nitrate hexahydrate (99.999% trace metals basis), nitric acid (ACS reagent, 70%) were purchased from Sigma-Aldrich. Millipore deionized water (18.2 MΩ cm) was used to prepare the slurries and solutions. A 15% wt. slurry was prepared by mixing 3 g zirconia powder, and 20 ml of DI water. By adding several drops of 0.1 M nitric acid, the pH of the slurry is adjusted to 4. The slurry was well mixed by using a stirring bar at 800 rpm for 30 minutes. After one end of the tube is sealed using a valve, the prepared slurry is transferred into the tube by glass pipet. The residual slurry is removed slowly after letting sit for 2 hrs and the valve is disconnected from the tube. The coated tube was then dried for 24 hrs at room temperature, followed by calcination at 500℃ for 4 hrs.

The zirconia layer was then impregnated with nickel to provide catalytic activity by filling the tube with 0.5 M nickel nitrate solution and letting sit for 2 hrs. Next, the solution was drained and the tube was dried for 24 hrs at room temperature, followed by calcination at 500℃ for 4 hrs.

The above steps (slurry coating and wet impregnation) were repeated 2 to 4 times to obtain the desired weight of the catalyst (0.05-0.1 g).

3.3 Analysis of reactant and product Gases

In this work, two different reactions are utilized to determine the catalyst activity. One is CO_2 Methanation, and the other is steam methane reforming. Prior to activity measurements, the prepared catalyst is reduced at 650℃ for 1 hr in a lab-scale tube furnace under a total gas flow of 130 sccm with a composition of 25 vol % H_2 in He.

For CO_2 Hydrogenation, ultrahigh purity He (99.999%), H_2 (99.999%), and CO_2 (99.999%) were purchased from Airgas and mixed and introduced into the reactor as reactants. Feeding flowrates of 30, 30, and 15 sccm were used for He, H_2 and CO_2, respectively. The reaction was performed under three different temperatures (350^{o}C, 450^{o}C, and 550^{o}C) display the relationship between temperature and the catalyst activity. Analysis of the reactants and products (CH_4, CO, H_2, and CO_2) was carried out through the detection and quantification of products using a gas chromatogram (Agilent 7890 GC system with TCD/FID).

For Steam Methane Reforming, ultrahigh purity He (99.999%) and CH_4 (balanced by 10% Mole Argon) were mixed with steam using water injected into preheated lines by a syringe pump. Feed flowrates of methane and He were set at 15 and 30 sccm, respectively. 22 μL/min of water was injected to provide a 2.5 molar ratio of steam/methane. The reaction was carried out under three different temperatures (650^{o}C, 750^{o}C, and 850^{o}C) to determine the relationship between temperature and the catalyst activity. The gas chromatograph (Agilent 7890 GC system with TCD/FID) was also utilized to detect the reactants and products (CH_4, CO, H_2, Ar, and CO_2).

Joule heating of the reactor tube or external heating by a tube furnace was used to provide heat for both CO_2 methanation and SMR. The temperature was changed by adjusting the current from the power supply for Joule heating, or the temperature controller for the furnace. Before each testing, the reactant mixture is analyzed by GC to determine the initial composition of the reactant gas stream at zero conversion. Under each set of conditions, at least 3 consecutive GC measurements were performed under each temperature mentioned above.

3.4 Description of the testing system

An existing bench scale reactor system shown in Figure 3.4.1 was used for all reaction experiments. This system allows the control of multiple gas feeds (He, H_2, CO_2, CH_4 and steam), supplies the heat for reaction and allows the analysis of the products through an on-line GC. He, H_2, and CO_2 were used for CO_2 methanation. He, CH_4 and steam were used for SMR. All gas flowrates were controlled by MKS model-G Mass Flow Controllers (MFC). Tubing before and after the reactor was pre-heated by heat tapes to 120℃ to prevent steam condensation. Fiberglass fabric strips were used as insulation for heating tapes to reduce heat loss.

The FeCr alloy tube reactor was connected into the testing system and was positioned inside the tube furnace. The tube furnace was only utilized as insulation layer when Joule heated reactor was tested. A Chroma model 62012P-40-120 DC power supply capable of supplying up to 40V, 120A and 1200W was used to control Joule heating of the reactor tube. To monitor the temperature of reactor, one K-type thermocouple was attached to the outer surface of the alloy tube. All gas reactants and products were analyzed by GC and then released to the vent system while steam was removed before the GC by a condenser.

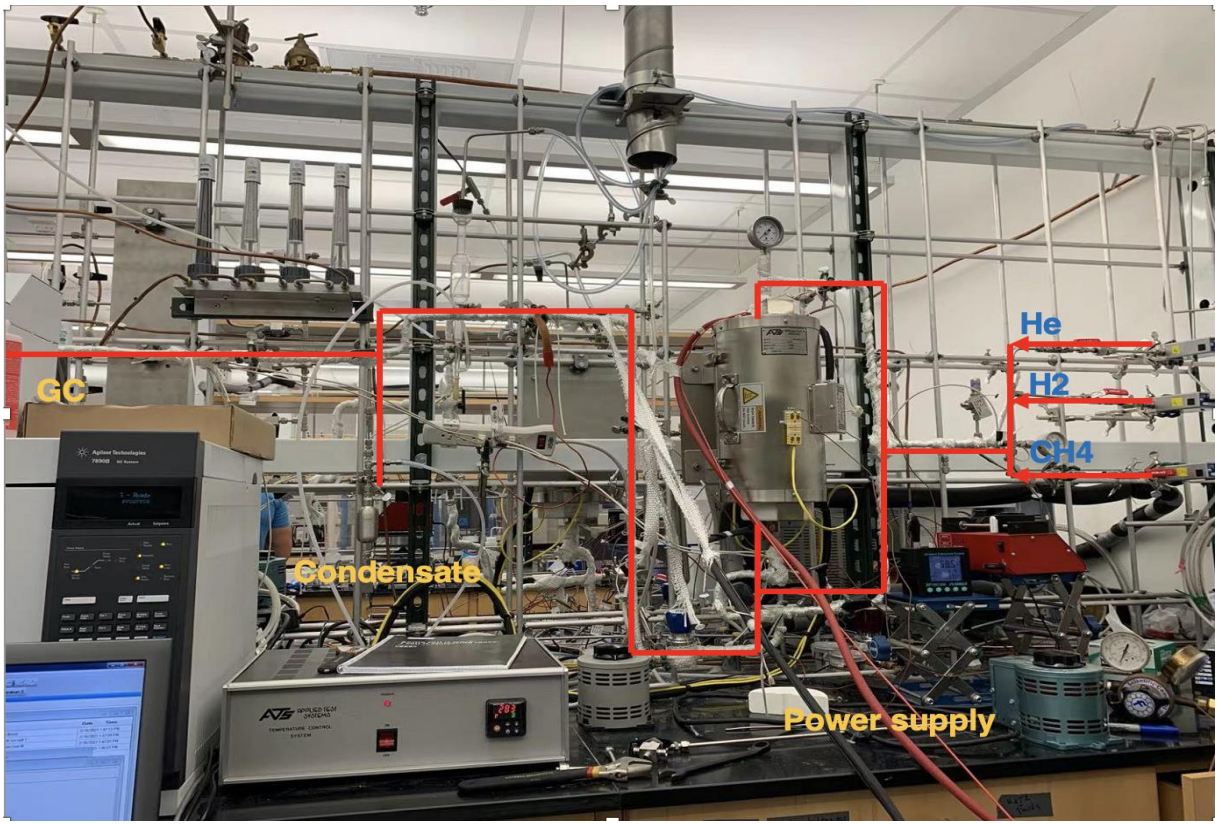

Figure 3.4. 1. Entire reaction set-up including gas inlets, reactor, power supply, condenser and GC in the Simonetti lab.

4. Results and Discussion

4.1 Joule heating

Initial heating tests were conducted when Joule heating the reactor tube before testing in the reaction setup. This was done to understand the behavior of the tube when under Joule heating. Initial experiments were intended to investigate if any sort of temperature profile exited along the length of the tube. Figure 4.1.1 shows the multiple positions (P1, P2 and P3) over the reactor for temperature measurement during initial Joule heating experiments. The heating experiment showed a decreasing trend in the temperature profile from the midpoint of the tube (P1) to both outer points when wrapped in insulation. Temperatures measured at P2 and P3 are similar but noticeably lower than P1. This was likely due to the two open-ends of the tube experiencing increased heat loss from the exposed ends of the tube when wrapped in insulation. During reaction

test this could result in uneven heating for catalysts. To test what effect this might have on the catalyst activity, a later set of experiments removed a section of washcoat from each end of the tube and compared its performance to tubes that did not have this section removed.

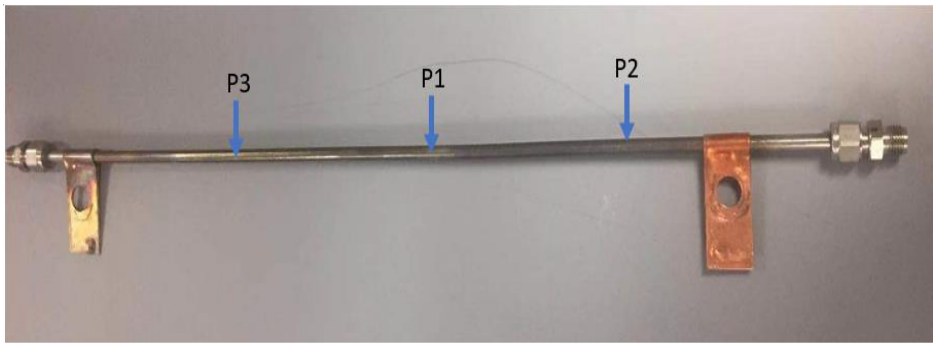

Figure 4.1. 1. Joule heated tube reactor with multiple testing position (P1: midpoint, P2 and P3: outer points) for thermal measurements.

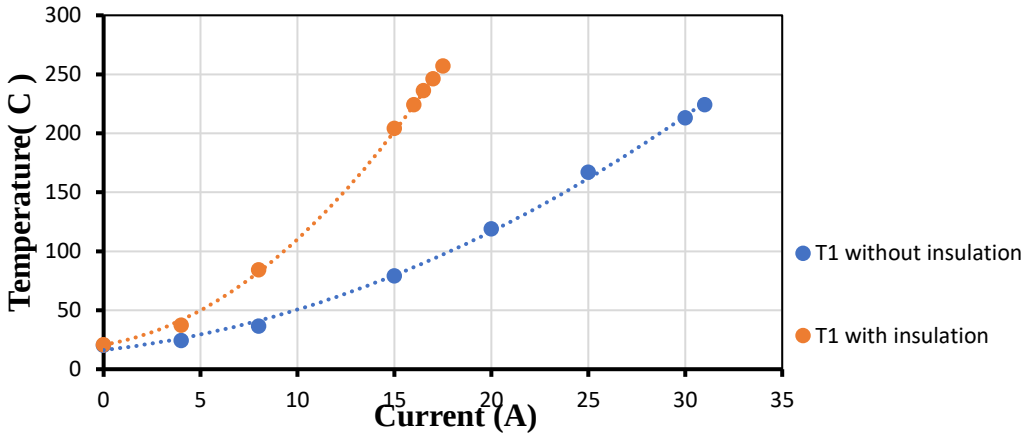

Figure 4.1. 2. Temperature vs. current curves for initial heating test on a Joule heated tube, blue points are temperature measured without insulation, orange points are temperature measured with insulation.

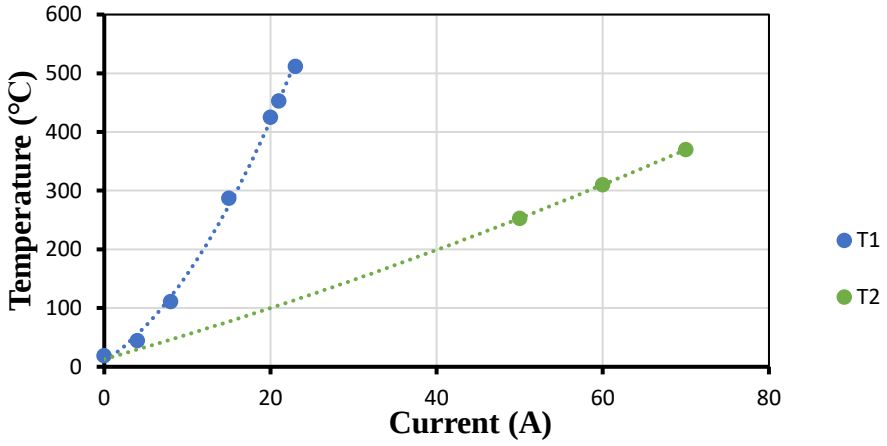

Figure 4.1. 3. Temperature vs current curves for initial heating test on a Joule heated tube, T1 is temperature measured on a Joule heated reactor in fume hood, T2 is temperature measured on a Joule heated reactor in furnace test system (Figure.3.4.1).

To obtain adequate heating performance from Joule heating, the effects of insulation, gas flowrate and external electrical circuits needed to be taken into account. As Fig.4.1.2 shown, Joule heating with insulation requires lower currents compared to Joule heating without insulation at the same temperature. The experiments conducted at higher temperature showed larger deviation between the temperature profiles. The results indicate the need for insulation to attain higher temperatures. Further testing was conducted while the reactor tube was installed inside the furnace system (Figure. 3.4.1). In Fig. 4.1.3, the initial test with Joule heating inside the furnace insulation (without any modification) was also studied for comparison with temperature tests in the fume hood. As shown in Fig.4.1.3, the temperature profiles decrease significantly in the furnace system and require more current input to achieve desired temperatures for Joule heating. To address this issue, modifications were made to the furnace system such as installing a PTFE section in the bypass to eliminate external circuits that drew current away from the reactor tube (Detailed modifications have been outlined in Derek Richard's thesis). With a better understanding of the

relationship between current and temperature during the Joule heating process, it was feasible to estimate the current for a desired temperature in the future reaction-based experiments.

4.2 Optimization of washcoating to stainless steel tubes

Although wet-impregnation and slurry coating are well-known processes, these techniques had not been previously used in the Morales-Guio lab. Thus, literature was referenced to attain initial procedure steps and optimization was conducted to determine the best method of producing washcoated reactors in this lab. Initial coating attempts utilized stainless steel (SS) tubes to determine important parameters for producing tubes with uniform coating layers. The coating parameters of tube length, slurry concentration and coating times, were taken into account. The following figures reveal the relationship between the material loading and the above coating parameters.

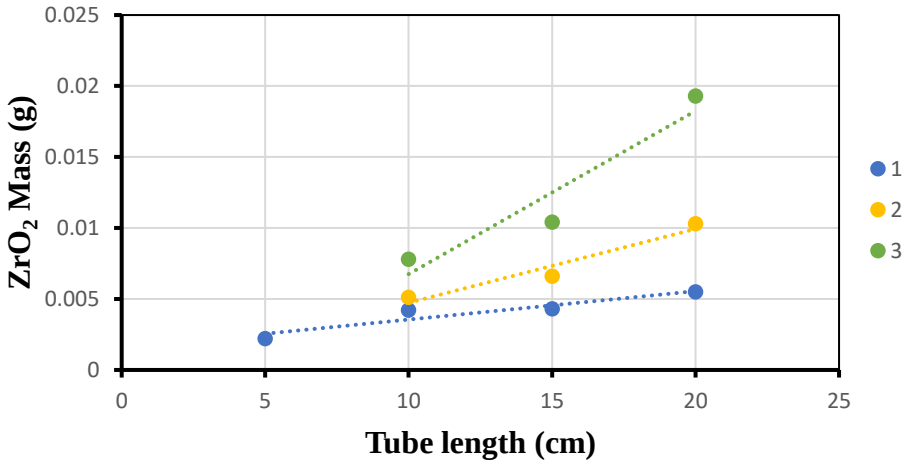

Figure 4.2. 1. ZrO_2 loading changing with tube length and number of coatings. 1 corresponds to one time coating and 2 and 3 corresponds to the repetition of the coating procedure two and three times, respectively.

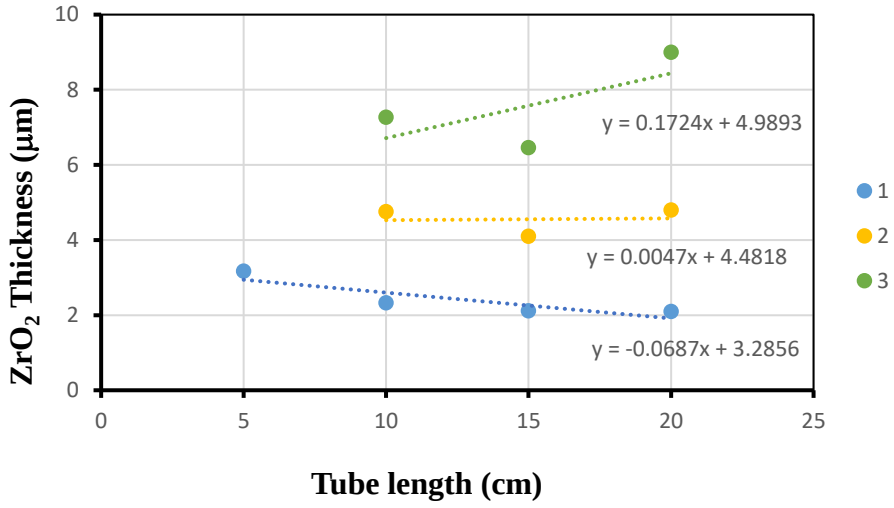

Figure 4.2. 2. Overall thickness of zirconia layer in steel tube. (The thicknesses are calculated based on the zirconia weight, assuming a porosity and finding what the theoretical thickness would be if evenly coated over the entire tube inner surface.) 1, 2, and 3 indicates the overall thickness of zirconia with one-, two-, and three-time coatings, respectively.

Figure 4.2.1 shows that the zirconia loading increases with the tube length and number of coatings. To estimate the coating thickness, the mass loading was divided by the inner surface area of the tube. Figure 4.2.2 shows the first two coating has similar thickness addition, but third coating showed a larger increase in additional zirconia. The increase in loading associated with the third coating is likely due to better metal oxide/metal oxide interactions in the presence of previous coats compared with tube surface/metal oxide interaction in the first two coatings. However, more coating times and increased mass loading increase particle conglomeration leading to more unstable and brittle washcoats. Since the attractive force between tube wall and metal oxide cannot bear the weight of zirconia entirely, it is susceptible to losing part of the mass loading in any following coating steps.

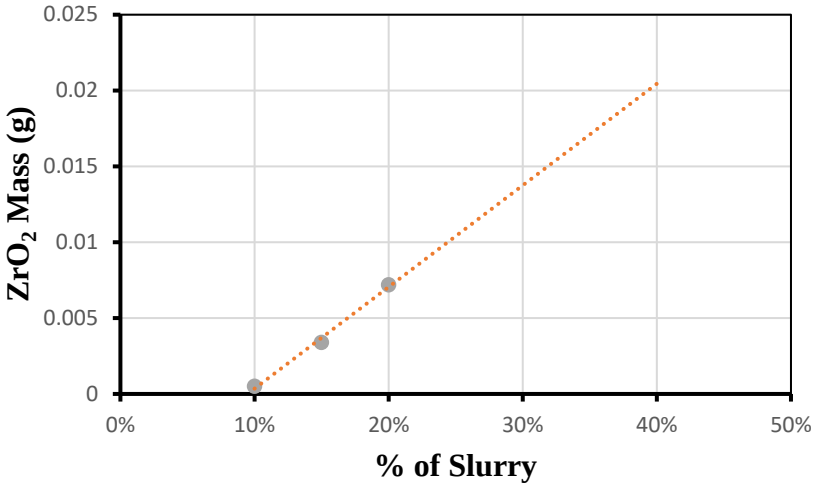

Figure 4.2. 3. ZrO_2 loading vs slurry concentration.

Additionally, physical properties of the slurry such as concentration and pH have significant influence on mass loadings. The mass loading is proportional to the concentration of slurry as shown in Figure 4.2.3. Within the concentration range of 10%-20%, the mass loading of zirconia increase concomitantly with increasing concentration of slurry. Obviously, high concentration means more particles contacting with tube surface at same time during coating process and would result in more particle residue over surface. Furthermore, pH also affects slurry viscosity and pH 4 was utilized for zirconia slurries due to the fact that this pH will result in the largest zeta potential of zirconia particles as previously discussed. To test what affect this might have on the catalyst activity, a later experiment tested coating a tube without pH adjustment in slurry and compared its performance to a tube with pH adjustment.

4.3 Catalysts Characterization

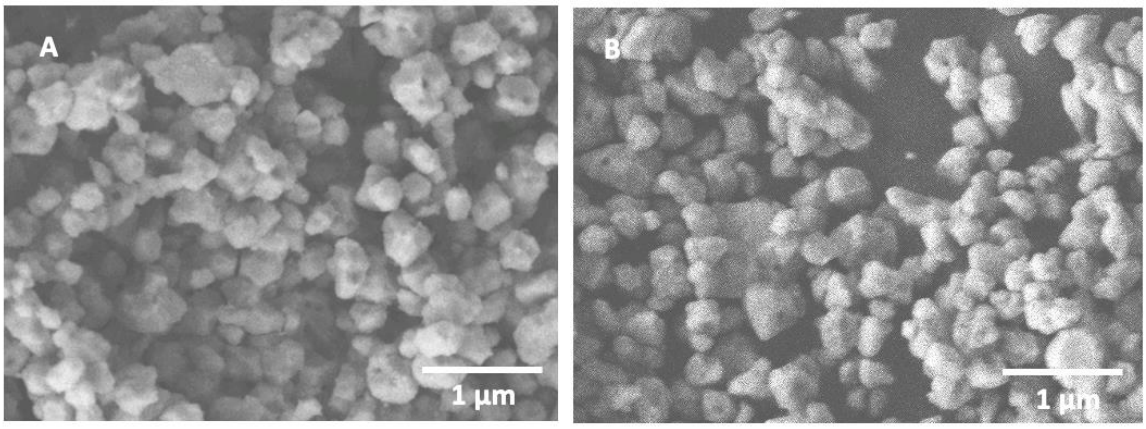

Figure 4.3. 1. Comparison of SEM images of Ni/ZrO_2 catalysts removed from stainless steel tube (A) and FeCr alloy tube (B)

Scanning electron microscopy (SEM) was used to examine the catalysts taken from the coated tube to investigate the surface morphology of the washcoated catalyst. These SEM images shown in Figure 4.3.1 show identical morphology and microstructure on two different materials of tubes: 6 (stainless steel) and 7 (alloy). The catalysts preparation procedures are identical for both tubes(tube materials and details, see Table 1). In the ZrO_2-supported catalyst, the zirconia can be seen with an aggregated form while nickel particles cannot be identified by SEM images. The supported zirconia catalysts show the porous microstructure which contribute to catalytic sites to gas transport during reaction process and the similarity in morphology suggests that there is no difference in the washcoat's structure between the stainless steel and FeCr Alloy tube.

4.4 CO_2 Methanation with various coated stainless-steel tubes

Multiple stainless-steel tubes and an FeCr alloy tube were washcoated for CO_2 methanation. Table 1 provides detailed preparation parameters for each tube, such as nomenclature, tube

material, number of coatings, heating methods, washcoat loading and whether washcoat was removed from the end of the tube or not.

Table 1. Multiple tubes were prepared by different parameters including number of coatings, tube materials, catalysts loading, removed end catalysts, heating method and nomenclature in this study.

Tube #	Number of coatings (Zirconia)	Tube Material	Removed End Catalysts (cm)	Heating Method	Washcoat Loading (g)	Nomenclature
1	1	SS	0	Furnace	-	Ni/ZrO_2(x1)/SS/0
2	1	SS	0	Furnace	0.0899	Ni/ZrO_2(x1)/SS/0
3	4	SS	0	Furnace	0.345	Ni/ZrO_2(x4)/SS/0
3R	4	SS	5	Furnace	0.115	Ni/ZrO_2(x4)/SS/5
4	4	SS	0	Furnace	0.0812	ZrO_2(x4)/SS/0
5	4	SS	0	Furnace	0.3695	Ni/ZrO_2(x4)/SS/0
6	2	SS	5	Furnace	0.0291	Ni/ZrO_2(x2)/SS/5
7	2	FeCr	5	JH	0.075	Ni/ZrO_2(x2)/FeCr/5

Annotation: For context in Nomenclature column of Table 1, Ni denotes deposition of nickel, ZrO_2(xN) denotes N number of zirconia coating, SS (stainless steel) or FeCr (Alloy) denotes tube materials, 0 or 5 denotes removing length of washcoat.

Fig. 4.4.1 shows the catalytic performance of tube 1 and 2 for CO_2 hydrogenation (Tube 1 (Ni/ZrO_2(x1)/SS/0) did not have pH adjustment and tube 2 (Ni/ZrO_2(x1)/SS/0) had pH adjustment during slurry deposition). CH_4 and CO are the two main products from this reaction and their production rates are used to demonstrate pH effects on catalyst activities. The result shows that pH adjustment in slurry preparation significantly improves methane production rates, while CO appears to be unaffected by adjustments made to the pH during slurry deposition. This is likely

due to the effect that pH has positive influence on the dispersions of nickel catalysts in zirconia support. The suitable pH would create better dispersion of the catalyst and produce more active sites to increase production of methane from either direct CO_2 methanation or CO hydrogenation. As Fig. 4.4.1B shown the production of CO seems to be the same due to limited hydrogen adsorbed by catalytic sites. The most of hydrogen would participate in CO hydrogenation step to form methane, but the amount of hydrogen is limited compared to CO. Therefore, it shows the similar CO production rate but large change in methane production.

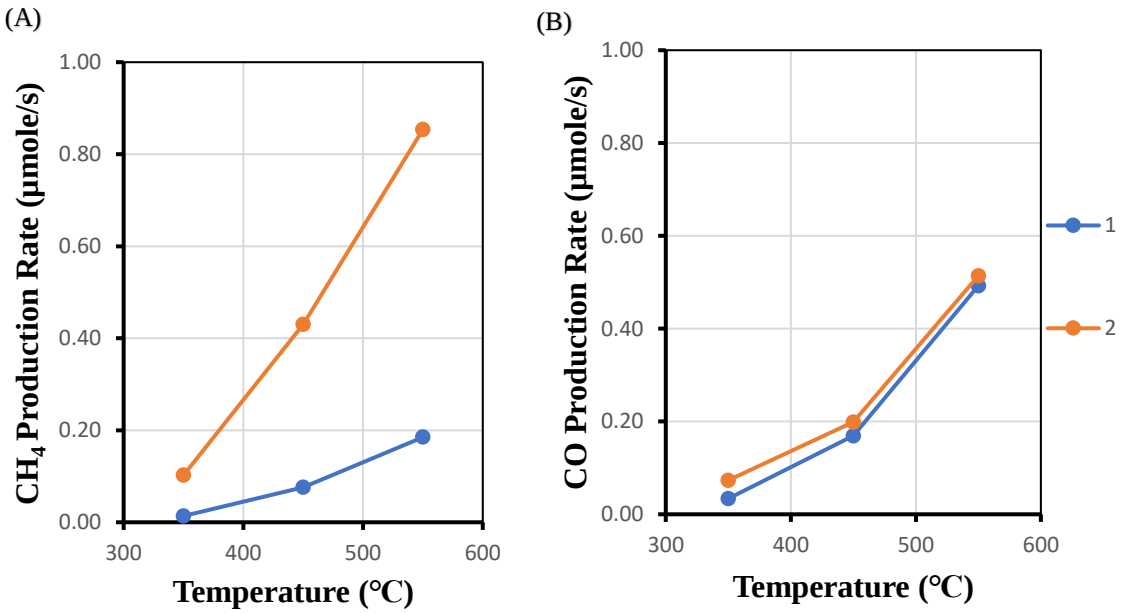

Figure 4.4. 1. Production rates of CH_4 (A) and CO (B) vs. temperature for comparison between stainless steel tube 1 and 2.

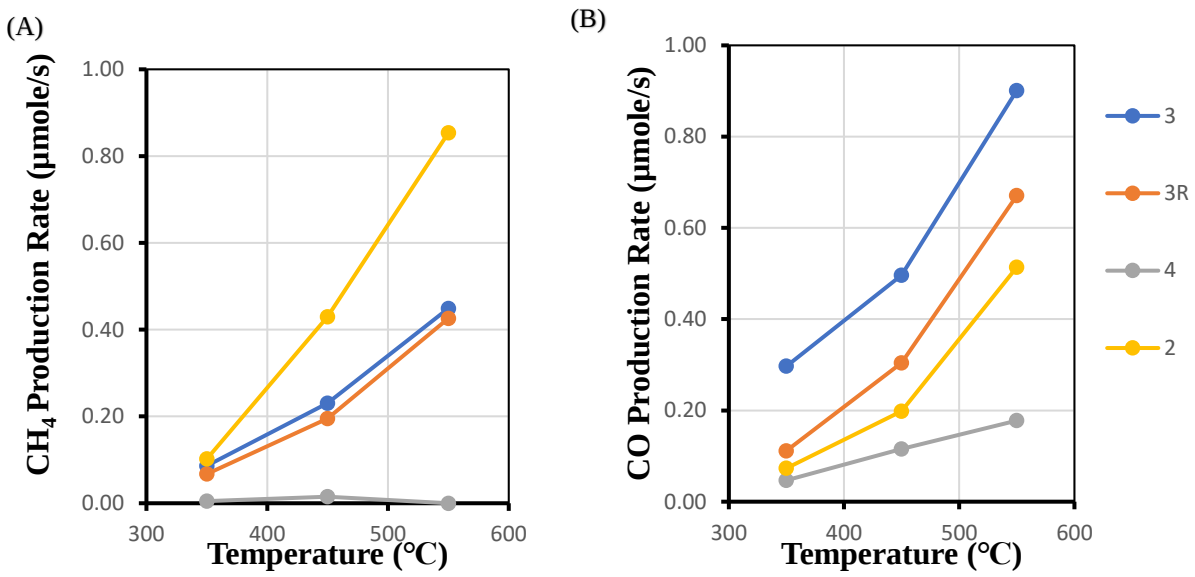

Figure 4.4. 2. CH_4 (A) and CO (B) production rate vs. temperature for comparision of various stainless steel tubes. (Tube # 2,3,3R, and 4, related preparing information in Table 1)

In Figure 4.4.2, CH_4 and CO production rates have been compared in various tubes (tube 2 ($Ni/ZrO_2(x1)/SS/0$), 3 ($Ni/ZrO_2(x4)/SS/0$), 3R ($Ni/ZrO_2(x4)/SS/5$), and 4 ($ZrO_2(x4)/SS/0$)) with different preaparation parameters. Tube 4 (zirconia support only), which is used as a control experiment, in comparison of other tubes (2, 3, and 3R) where nickel has been deposited on the zirconia support. Obviously, tube 4 shows little to no activity as expected. The production differences among those tubes are caused by the presence of nickel particles and increased temperature. Moreover, tube 2 has one fold higher methane production rates, but it has a 0.255 g lower washcoat loading than tube 3. This reduced activity is caused by a higher washcoat loading which results in higher mass transfer limitations. That is, reactants need to pass through longer pathways to reach catalytic sites. The differences in selectivity and normalized methane production rate between tube 2 and 3 (Fig. 4.4.3) comfirm that less coating times and thinnner layer of washcoated catalysts seems to be better options for maximizing methane yield.

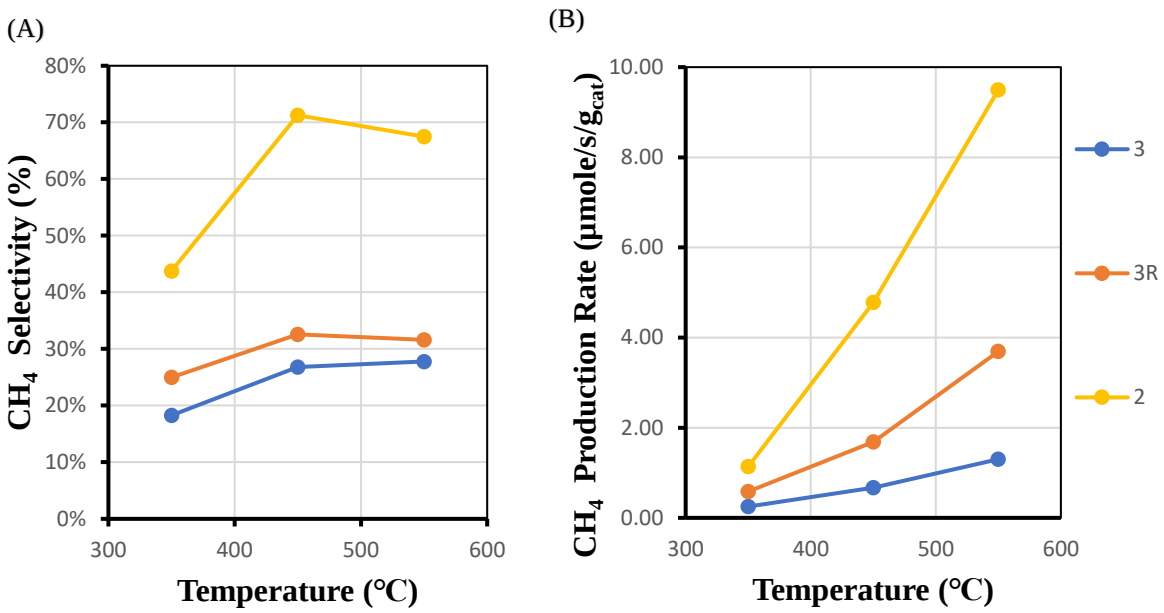

Figure 4.4. 3. CH_4 selectivity (A) and nomarlized production rate (B) vs. temperature on various stainless steel tubes with different thicknesses of washcoat.

Tube 3 (Ni/ZrO_2(x4)/SS/0) and 3R (Ni/ZrO_2(x4)/SS/5) are the same tube. However, tube 3R was tested in a separate experiment after 5 cm of washcoat (67% of overall loading) had been removed from both ends of tube 3. As shown in Figure 4.4.2A, methane production rates on tube 3R shows little variation compared with Tube 3, which means the catalysts on the ends of tube do not have large contribution to the CO_2 reactions. For normalized methane production rates (Fig 4.4.3B), tube 3R displays higher value than tube 3 which cannot be seen in Figure 4.4.2A. The less coating has higher normalized reaction rates and it further comfirms that the removed catalysts are not contributing significantly to the reaction. CO production rates on tube 3R, on the other hand (Figure 4.4.2B), shows 50% decrease compared with Tube 3. This behavior could be due in part to the fact that the two ends of the tube are not insulated as well as the rest of the tube and therefore there is a temperature gradient from middle to end of tube for CO_2 methanation. The temperature gradient, athough small, could lead to the catalysts at the end of the tube being less active for CO

hydrogentaion (yeild CH_4 from CO). Methane selectivity (Fig. 4.4.3A) for tube 3R is slightly higher than tube 3. One reason is the removal of catalytic sites on tube ends along with a tiny methane production rate change. Another reason could be the temperature gradient described previously. The reduced CO production rates and almost unchanged methane prouduction rates in tube 3R may result in the selectivty change.

4.5 **Comparison between external heating and Joule heating**

The primary purpose of investigating washcoat parameters was to utilize this information in fabricating a wahscoated FeCr Alloy tube for Joule heating. The alloy tube's washcoat loading was targeted to be comparable to tube 2 ($Ni/ZrO_2(x1)/SS/0$) and the washcoat was removed from the ends of the alloy tube to maximize methane yield. In testing, this tube was also Joule heated in contrast to the stainless steel tubes which were heated by the furnace.

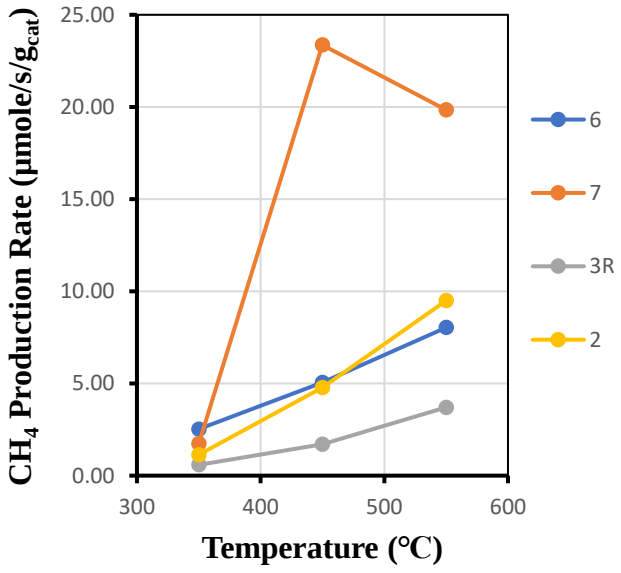

Figure 4.5. 1. Normalized methane production rate vs. temperature for comparing FeCr alloy tube (7) with various stainless steel tubes (2, 3R, 6) with different thickness of washcoat.

In Fig 4.5.1, normalized methane production rates are investigated for different tube materials. Tube 7 (Ni/ZrO_2(x2)/FeCr/5) has much higher methane production rates than tube 6 (Ni/ZrO_2(x2)/SS/5) which indicates Joule heating process is more effective than furnace heating. As temperature increases from 350℃ to 450℃, tube 7 displays a significant increase in methane production rate and reaches the maximum rates at 450℃. Compared with tube 6, tube 7 has entirely different trends that is most likely because the reaction happening in the tube is kinetic control instead of mass transfer control. At 450℃, methane equilibrium concentration is 0.39 mol/s, which is much higher than our actual reaction rate, 1.64×10^{-6} mol/s. The huge difference in concentration indicates the reaction is transport or kinetically limited rather than thermodynamically limited. Furthermore, comparison of tube 2 (Ni/ZrO_2(x1)/SS/0), 3R (Ni/ZrO_2(x4)/SS/5), and 6 (Ni/ZrO_2(x2)/SS/5) are studied to estimate the relationship between coating times and catalysts performance. Normalized methane production rates on tube 2 (one coating) and tube 6 (two coatings) shows little variation (less than 10%), while tube 3R shows a drop in the methane production rate. This phenomenon implies that a larger number of coatings would decrease the catalytic performance significantly. Sebastian et al.[13] stated the catalytic effectiveness factor depends on internal diffusion through catalysts. The diffusion performance would increase by having a lower washcoat thickness. Therefore, the catalytic effectiveness factor increased by decreasing the washcoat layer thickness.

To prove whether tube 7 (Ni/ZrO_2(x2)/FeCr/5) is under kinetic control, two estimated activation energies were calculated by Arrhenius equation and the value are listed in the table 2 (Detailed calculations and plots are shown in Appendix. B). In this table, one is based on CO_2 consumption rate which represents overall reaction activation energy, and the other is the individual reaction activation energy for methane production. Tube 7 shows highest methane

activation energy 54.3 kJ/mol which indicates a transition stage from mass transfer to kinetic control. The higher value is caused by promoted catalyst activity resulting in more methane generation. Compared with the value, 82.8 kJ/mol observed by Charlotte et. al[39], all three tubes have a lower CO_2 activation energy (less than 30 kJ/mol). All those low values indicate insufficient catalyst loading and rates affected by mass transport. The low loading leads to insufficient catalytic activity for CO_2 methanation. Therefore, more efforts can be put to increase catalyst loading in the future.

Table 2. Calculated activation energy for tube 6 (Ni/ZrO_2(x2)/SS/5), 7 (Ni/ZrO_2(x2)/FeCr/5) and 3R(Ni/ZrO_2(x4)/SS/5).

Tube #	CO_2 (kJ/mol)	CH_4 (kJ/mol)
3R	34.0	28.1
6	27.7	24.7
7	28.9	54.3

Overall, the most interesting observation from the use of Joule heating for CO_2 hydrogenation was the significant increase in methane production and the detection of other reduction products, such as ethane. Two possible hypotheses are proposed to explain these observations. First, it is because the thermal gradient mentioned in section 2.1. Second, the passing of a current through the Joule heated tube may be affecting the catalyst by electrochemical interactions although it is unclear how this might happen considering that ZrO_2 is a highly resistive material. After applying around 3V potential to the tube, some electrons may pass through the washcoated catalysts. The negative charges may change the potential of catalysts surfaces and the excess charge could activate nickel sites. The potential difference between solid phase and gas phase may shift toward a predictable equilibrium value given by the Nernst equation. During that

equilibrium process, transfer of charge may promote the CO_2 methanation. However, there is no clear evidence proving whether the electrons pass through catalysts or not. Future experiments should seek to understand what causes Joule heating to improve the performance of these tubes.

4.6 Steam Methane Reforming

The washcoated catalysts in Tube 6 (Ni/ZrO_2(x2)/SS/5) and 7 (Ni/ZrO_2(x2)/FeCr/5) were tested under SMR for further study on catalyst activity. The results of the experiments demonstrates that tube 6 has less than 10 % methane conversion which shows the low catalytic activity due to the thermal gradients in the tube reactor with external heating. In contrast, tube 7 has a significant increase on catalytic activity and the methane conversion is over 95% at 750℃. The 100 folds difference of hydrogen production rates (Fig. 4.6.1B) indicates that Joule heating is better than external heating at 750℃.

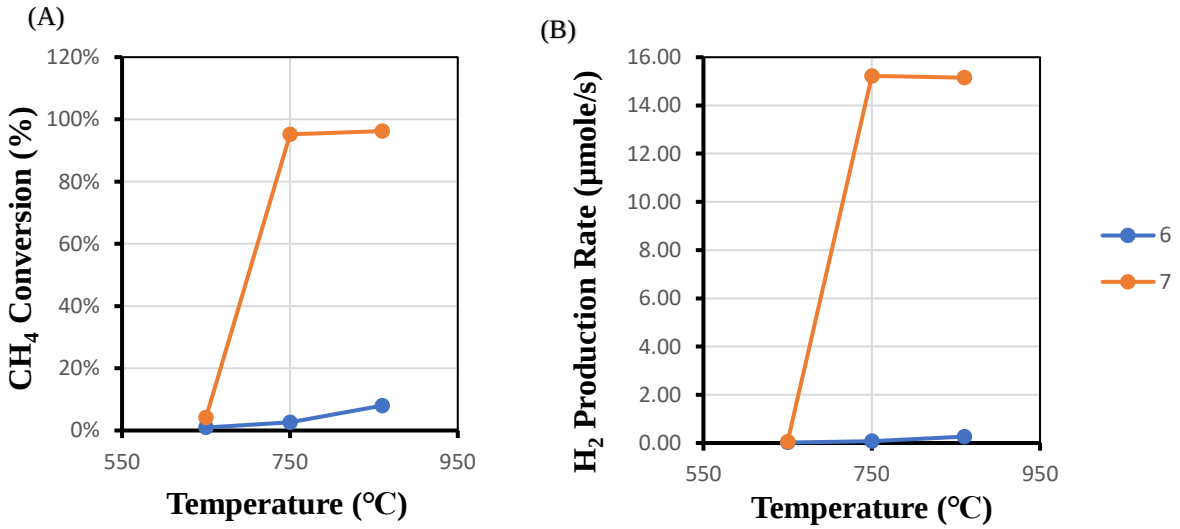

Figure.4.6 1. CH_4 Conversion (A) and H_2 production (B) vs. temperature for comparison between stainless tube 6 and FeCr alloy tube 7

Our maximum hydrogen production (around 1.55×10^{-5} mol/s at 850℃) which is 46 folds lower than the value (7.4×10^{-4} mol/s at 1015℃) observed by Sebastian et. al.[13] Operating

temperature, washcoat thickness, and hydrogen feeding flowrates are possible factors result in the huge difference in hydrogen production. First, SMR is more preferred at higher temperature due to its endothermicity. Second, more catalytic sites will produce more hydrogen. Finally, hydrogen (fed as reactant) has positive effects on catalyst performance. If the H_2/H_2O ratio exceeds the equilibrium constant for nickel reduction, the reduction of the nickel oxide will occur. Thus, the presence of hydrogen would reduce the oxide and keep nickel in active state during SMR.[40]

During Joule heating experiment with tube 7 (Ni/ZrO_2(x2)/FeCr/5), the methane conversion was decreasing over numbers of GC injections. Since the current was changed over time to maintain constant reactor temperature, it was unclear whether current or catalyst degradation led to decrease conversion or not. To verify if the current is related to catalytic performance, multiple injections of products for SMR were taken at 850℃ with fixed current. As shown in Figure 4.6.2, methane conversion is decreasing at fixed current during the process. Catalyst degradation may contribute to this conversion reduction. Normally, coke formation happens at high temperature in SMR and will occupy catalytic sites to prevent further reactions. The coke formation is proved by carbon mass balance which reveals only 30% CH_4 are transformed into CO_2 and CO.

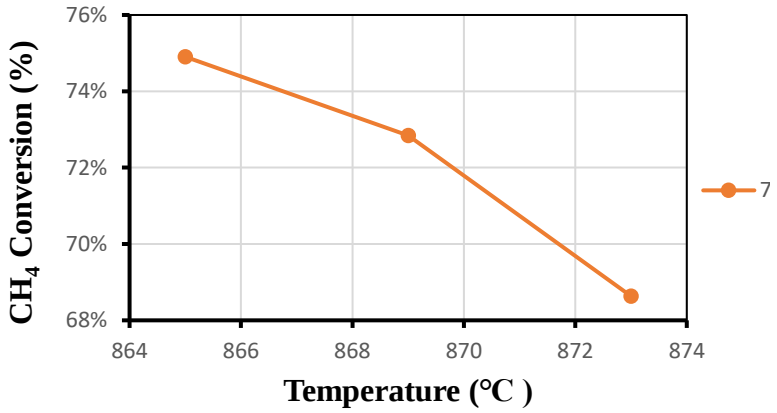

Figure.4.6 2. CH_4 conversion vs temperature for FeCr alloy tube 7 at fixed current.

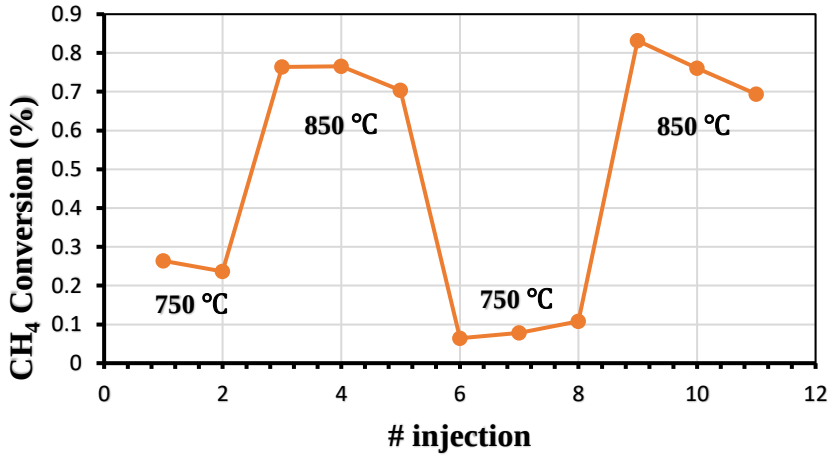

Figure.4.6 3. CH_4 conversion for FeCr alloy tube 7 observed at 750 ℃ and 850 ℃ with varying current.

To further investigate catalysts degradation, the tube 7 (Ni/ZrO_2(x2)/FeCr/5) is conducted with a step change in temperature between 750℃ and 850℃. Figure 4.6.3 shows temperature increased from 750℃ to 850℃, the methane conversion changed from 11% to 83%. The step change in conversion is because positive effect of the increasing temperature is overcoming the negative effect of deactivation mechanism. Obviously, the reaction rate is much higher at 850℃ than 750℃, since the reaction is under kinetic control. Compare conversion for both times at 750℃,

the second time (larger number of injection) is lower than the first. This means there is a deactivation mechanism, likely coke formation. When the temperature is decreased to 750℃ from 850℃ that decrease in activity is likely due to the production of methane from the coking being stripped. Further studies need to be researched to understand how current affect catalyst in this phenomenon.

5. **Conclusion and Outlook**

Growing concerns for the global climate change and energy requirements demand reconstruction on fossil fuel. Joule heating offers a new alternative to replace a large-scale endothermic process which reduce CO_2 emission and energy requirements. In this work, an existing Joule heated reactor was modified to investigate its effect on CO_2 methanation and SMR. A first step for constructing Joule heated reactor is to understand the catalytic washcoating process. pH, slurry concentration, and number of coatings are key parameters to adjust washcoat performance in the process. First, the specific pH value, 4 for Ni/ZrO_2 catalysts, has displayed a better performance of catalyst since the pH would increase the zeta potential of zirconia particles to have a better dispersion. Second, higher slurry concentration would has a higher washcoat loading on the tube due to more particles. Lastly, the deposition of the washcoat through multiple zirconia deposition process increases the thickness of the washcoat and the zirconia loading. However, the thick support would result in a longer pathway and higher internal mass transfer inside washcoat layers.

A stainless-steel tube reactor with external heating was used as a baseline compared with Joule heated alloy tube reactor. Their washcoated Ni/ZrO_2 catalysts were tested for CO_2 methanation and SMR, separately. For CO_2 methanation, the Joule heating method promotes

catalyst activity to have a higher methane production rate since it reduce thermal gradient. For SMR, Joule heating contributes to catalyst activity for and resulting in high methane conversion (95%). Coke formation was observed and led to catalyst degradation for SMR. However, Joule heating somehow can overcome the activity loss by increasing significantly in temperature. Overall, the Joule heating has a significant positive effect on the catalyst performance. However, it is still not clear what is reason behind Joule heating's performance enhancement.

Despite Joule heating potentially offering some advantages such as quicker reactor start-up and a reduction of CO_2 emission associated with the use of fired furnaces, the effect of improved heat transfer in catalysis and the effects that the applied potential can have on the catalyst activity and the system stability need to be studied further. In the short-term goal, the improvement of electrical contact and optimization of the washcoating process can be focused to improve Joule heated reactor efficiency. For example, the addition of organic binders (glycerol and polyvinyl alcohol) which can be used to enhance stability and viscosity of the slurry. Thermal pretreatment (>800℃) of the alloy tubes can enhance the catalysts adhesion over the tube's surface through the formation of thin surface oxide layers. In the long-term, more research efforts need to be dedicated to the understanding of the catalyst degradation. Sebastian et al.[13] shows the thickness of washcoat plays an essential role on catalytic effectiveness and indicates a thick coating (30 μm) can provide good resistance to deactivation. Moreover, Ru or Rh is an attractive metal which has higher intrinsic activity and better carbon resistance.[13] Combined them with nickel catalyst may be an alternative way to reduce catalysts deactivation.

Appendices

Appendix. A GC calibration

The concentration of gas products was calibrated by comparing the GC TCD sensor measurement with mass flow controller measurement. The following calibration curves (Fig A.1, A.2, A.3) are got for estimating concentration of H_2, CO_2, and CH_4 based on known volume fraction. The calibration parameter of CO is estimated by a single TCD sensor measurement from a standard gas (1% mole CO included). The low concentration would lead to a poor estimation on CO production rate.

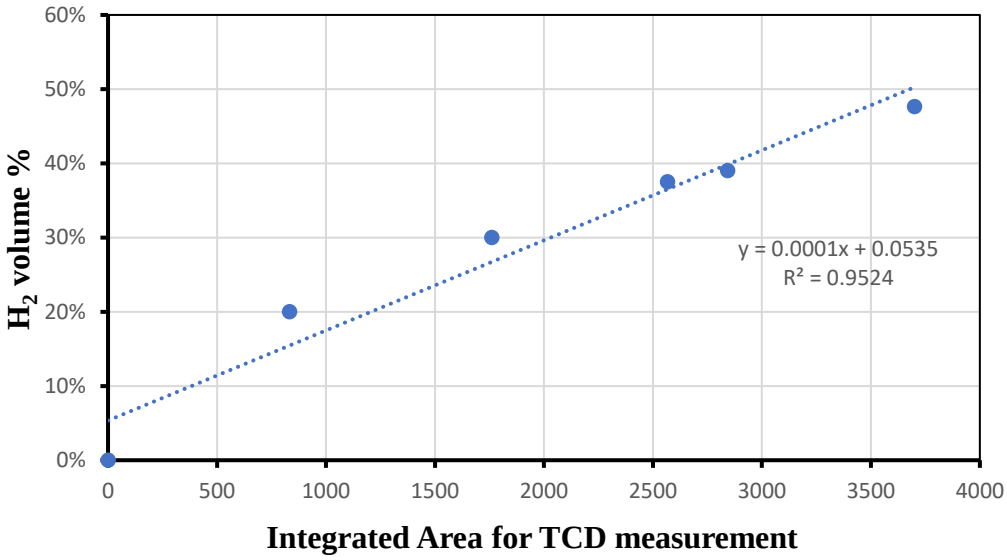

Figure A. 1. GC calibration curve for H_2.

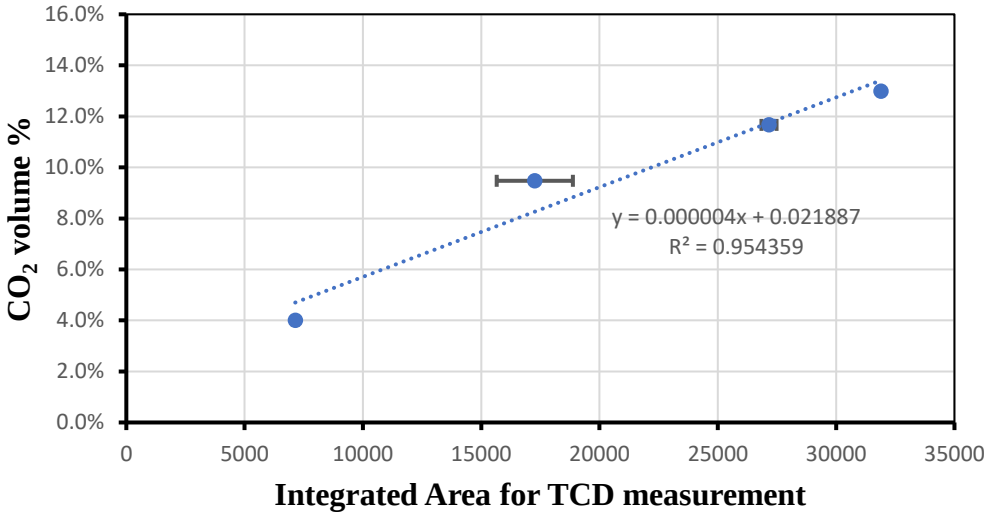

Figure A. 2. GC calibration curve for CO_2.

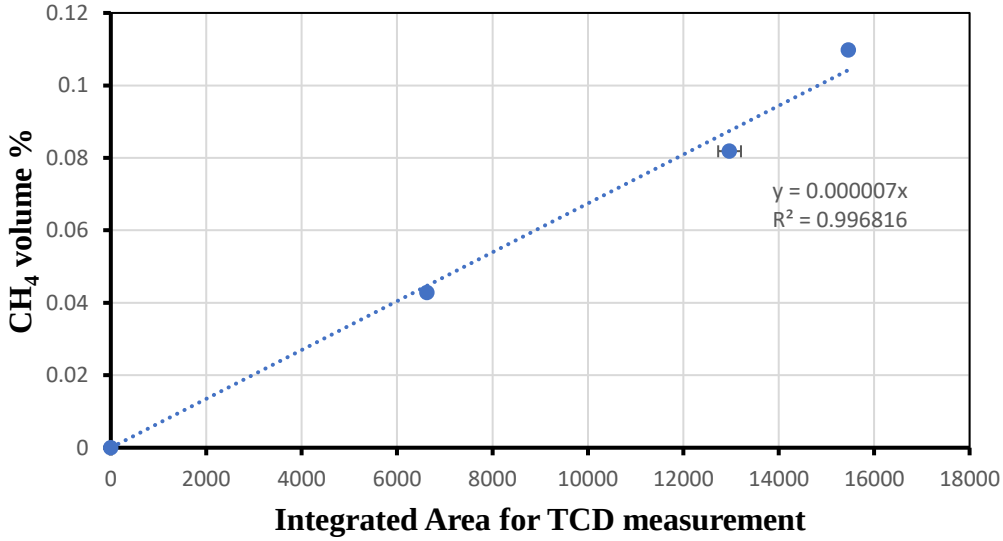

Figure A. 3. GC calibration curve for CH_4.

Appendix. B Activation Energy

The activation energy is calculated from the rearranged Arrhenius equation which is defined as the following steps. Taking logarithms on both sides Arrhenius equation (B-1) and nth order rate equation (B-2). Then, combining and rearranging them to get equation (B-3) which is used to determine the activation energy by plotting ln r vs.1/T. The plot will give a straight line whose slope is $\frac{-E_a}{R}$ (some examples are shown in Figure. B.1).

$$k = Ae^{-E_a/RT} \tag{B-1}$$

$$r = kC^n \tag{B-2}$$

$$\ln r = C' + (\frac{-E_a}{R})(\frac{1}{T}) \tag{B-3}$$

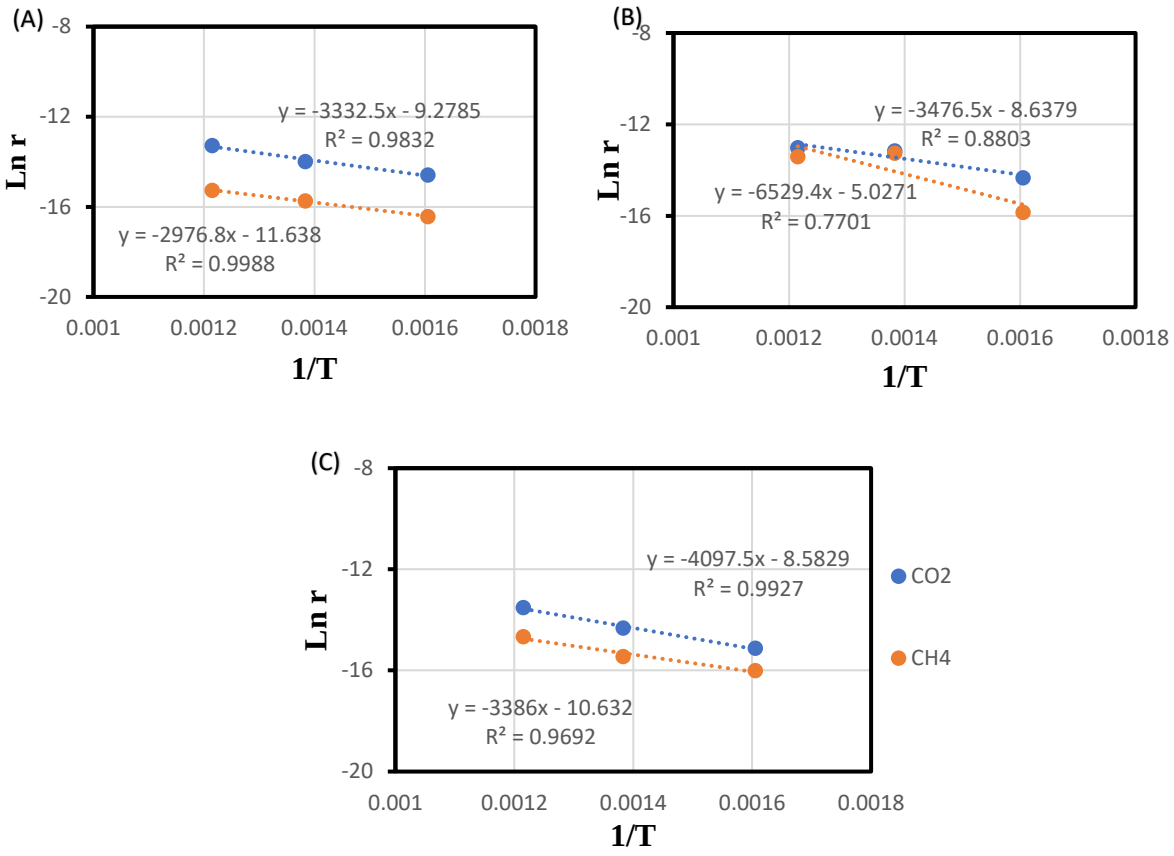

Figure B. 1. The Arrhenius plot of ln r as a function of 1/T, the calculated activation energy shown in Table 2, (A) is Tube 6 (Ni/ZrO_2(x2)/SS/5), (B) is Tube 7 (Ni/ZrO_2(x2)/FeCr/5), (C) is Tube 3R(Ni/ZrO_2(x4)/SS/5).

Appendix. C Supplementary Figures and table

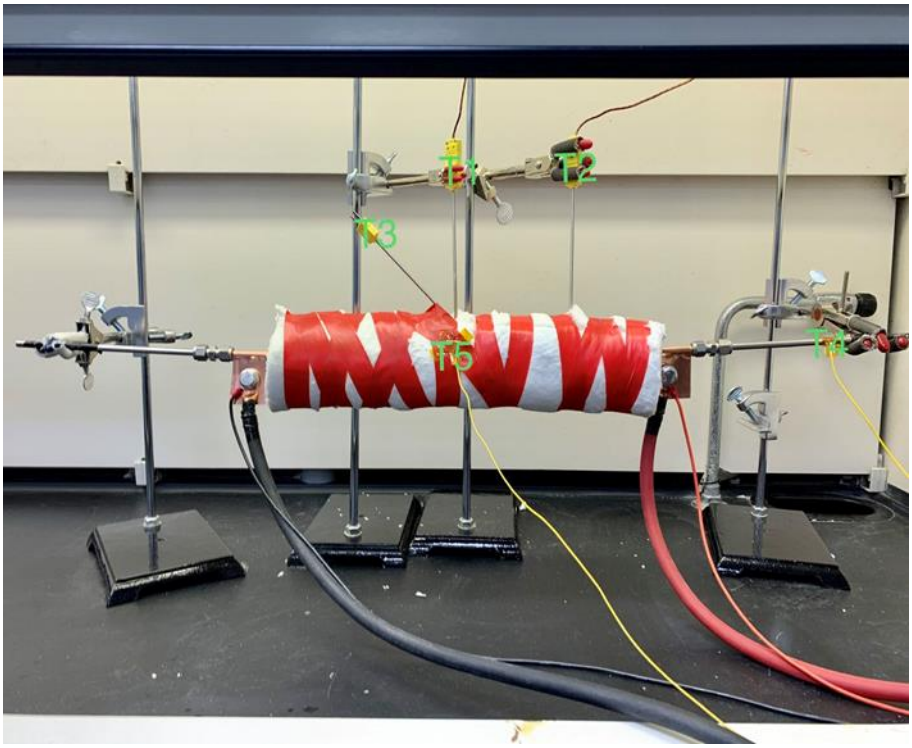

Figure C. 1. The initial heating set-up with labeled thermocouples.

Table 3. The measured temperature profile of experiment shown in Figure C.1.

Current (A)	Voltage (V)	Power (W)	T1 (℃)	T2 (℃)	T3 (℃)	T4 (℃)	T5 (℃)
0	0	0	19.1	19.2	19.8	19.2	19.2
4	0.414	1.656	44.7	42.9	42	20.1	19.2
8	1.14	9.12	111	105	108	19.8	25.3
15	1.74	26.1	287	268	280	19.8	31.2
20	2.25	45	425	397	411	20.1	34.1
21	2.34	49.14	453	422	439	20	37
23	2.63	60.49	512	479	499	20.1	45

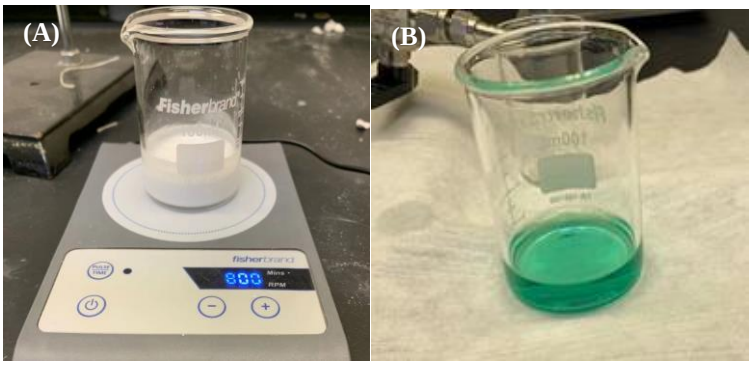

Figure C. 2. The prepared 15% ZrO_2 slurry (A) and 0.1 M nickel nitrate solution (B).

Figure C. 3. The nickel catalysts are well coated to steel tube, the light green powder contains zirconia and nickel.

References

1. Saunois, M. *et al.* The global methane budget 2000-2017. *Earth System Science Data* **12**, 1561–1623 (2020).

2. Sabine, C. *et al. Carbon and Other Biogeochemical Cycles. In: Cli-mate Change 2013: The Physical Science Basis. Contribution of Working Group I to the Fifth Assessment Report of the Intergovernmental Panel on Climate Change Coordinating Lead Authors: Lead Authors: Contributing Authors*. (2013).

3. Turner, A. J., Frankenberg, C. & Kort, E. A. Interpreting contemporary trends in atmospheric methane. *Proceedings of the National Academy of Sciences of the United States of America* vol. 116 2805–2813 (2019).

4. Solaun, K. & Cerdá, E. Climate change impacts on renewable energy generation. A review of quantitative projections. *Renewable and Sustainable Energy Reviews* vol. 116 (2019).

5. Owusu, P. A. & Asumadu-Sarkodie, S. A review of renewable energy sources, sustainability issues and climate change mitigation. *Cogent Engineering* vol. 3 (2016).

6. Iulianelli, A., Liguori, S., Wilcox, J. & Basile, A. Advances on methane steam reforming to produce hydrogen through membrane reactors technology: A review. *Catalysis Reviews - Science and Engineering* **58**, 1–35 (2016).

7. Moioli, E., Mutschler, R. & Züttel, A. Renewable energy storage via CO2 and H2 conversion to methane and methanol: Assessment for small scale applications. *Renewable and Sustainable Energy Reviews* **107**, 497–506 (2019).

8. García, L. Hydrogen production by steam reforming of natural gas and other nonrenewable feedstocks. in *Compendium of Hydrogen Energy* 83–107 (Elsevier, 2015). doi:10.1016/b978-1-78242-361-4.00004-2.

9. Bozzano, G. & Manenti, F. Efficient methanol synthesis: Perspectives, technologies and optimization strategies. *Progress in Energy and Combustion Science* vol. 56 71–105 (2016).

10. Zhou, L., Guo, Y., Yagi, M., Sakurai, M. & Kameyama, H. Investigation of a novel porous anodic alumina plate for methane steam reforming: Hydrothermal stability, electrical heating possibility and reforming reactivity. *International Journal of Hydrogen Energy* **34**, 844–858 (2009).

11. Rieks, M., Bellinghausen, R., Kockmann, N. & Mleczko, L. Experimental study of methane dry reforming in an electrically heated reactor. *International Journal of Hydrogen Energy* **40**, 15940–15951 (2015).

12. Zhang, Q. *et al. A 2D model for the cylinder methane steam reformer using electrically heated alumite catalyst*.

13. Wismann, S. T. *et al. Electrified methane reforming: A compact approach to greener industrial hydrogen production*. http://science.sciencemag.org/.

14. Rieks, M., Bellinghausen, R., Kockmann, N. & Mleczko, L. Experimental study of methane dry reforming in an electrically heated reactor. *International Journal of Hydrogen Energy* **40**, 15940–15951 (2015).

15. Zhou, L., Guo, Y., Yagi, M., Sakurai, M. & Kameyama, H. Investigation of a novel porous anodic alumina plate for methane steam reforming: Hydrothermal stability, electrical heating possibility and reforming reactivity. *International Journal of Hydrogen Energy* **34**, 844–858 (2009).

16. Zhang, D. The ductility below the ductile-to-brittle transition temperature of the FeCrAlloy. *Journal of Alloys and Compounds* vol. 479 (2009).

17. Liu, H. & Chen, W. Coke formation and metal dusting of electroplated Ni3Al-CeO2-based coatings in CO-H2-H2O. *Corrosion Science* **49**, 4134–4153 (2007).

18. Zhang, D. The ductility below the ductile-to-brittle transition temperature of the FeCrAlloy. *Journal of Alloys and Compounds* vol. 479 (2009).

19. Pauletto, G. *et al.* FeCrAl as a Catalyst Support. *Chemical Reviews* vol. 120 7516–7550 (2020).

20. Montebelli, A. *et al.* Methods for the catalytic activation of metallic structured substrates. *Catalysis Science and Technology* vol. 4 2846–2870 (2014).

21. Meille, V. Review on methods to deposit catalysts on structured surfaces. *Applied Catalysis A: General* vol. 315 1–17 (2006).

22. Valentini, M. *et al. The deposition of-Al 2 O 3 layers on ceramic and metallic supports for the preparation of structured catalysts*. *Catalysis Today* vol. 69 (2001).

23. Avila, P., Montes, M. & Miró, E. E. Monolithic reactors for environmental applications: A review on preparation technologies. *Chemical Engineering Journal* **109**, 11–36 (2005).

24. Cristiani, C., Visconti, C. G., Finocchio, E., Stampino, P. G. & Forzatti, P. Towards the rationalization of the washcoating process conditions. *Catalysis Today* **147**, (2009).

25. Balzarotti, R., Ciurlia, M., Cristiani, C. & Paparella, F. Washcoat deposition of Ni- and Co-ZrO2 low surface area powders onto ceramic open-cell foams: Influence of slurry formulation and rheology. *Catalysts* **5**, 2271–2286 (2015).

26. Agrafiotis, C., Tsetsekou, A. & Leon, I. *Effect of Slurry Rheological Properties on the Coating of Ceramic Honeycombs with Yttria-Stabilized-Zirconia Washcoats*.

27. Wu, D., Zhang, Y. & Li, Y. Mechanical stability of monolithic catalysts: Improving washcoat adhesion by FeCrAl alloy substrate treatment. *Journal of Industrial and Engineering Chemistry* **56**, 175–184 (2017).

28. Zhang, D., Zhang, L., Liang, B. & Li, Y. Effect of acid treatment on the high-temperature surface oxidation behavior of FeCrAlloy foil used for methane combustion catalyst support. *Industrial and Engineering Chemistry Research* **48**, 5117–5122 (2009).

29. Martínez Tejada, L. M., Domínguez, M. I., Sanz, O., Centeno, M. A. & Odriozola, J. A. Au/CeO2 metallic monolith catalysts: Influence of the metallic substrate. *Gold Bulletin* **46**, 221–231 (2013).

30. Xu, X. *et al.* Insights into CO2 methanation mechanism on cubic ZrO2 supported Ni catalyst via a combination of experiments and DFT calculations. *Fuel* **283**, (2021).

31. Su, X. *et al.* Catalytic carbon dioxide hydrogenation to methane: A review of recent studies. *Journal of Energy Chemistry* vol. 25 553–565 (2016).

32. Frontera, P., Macario, A., Ferraro, M. & Antonucci, P. L. Supported catalysts for CO2 methanation: A review. *Catalysts* vol. 7 (2017).

33. Saeidi, S., Amin, N. A. S. & Rahimpour, M. R. Hydrogenation of CO2 to value-added products - A review and potential future developments. *Journal of CO2 Utilization* vol. 5 66–81 (2014).

34. Liu, Z.-W., Jun, K.-W., Roh, H.-S. & Park, S.-E. *Hydrogen production for fuel cells through methane reforming at low temperatures The effects of O 2 :CH 4 and H 2 O:CH 4 ratios on the conversion of CH 4 , the hydrogen yield, the selectivity for carbon monoxide, and the H 2 :CO ratio are investigated at 650 8C with a constant CH 4 space velocity. Results indicate that CH 4 conversion increases signi®cantly with increasing O 2 :CH 4 or H 2 O:CH 4 ratio, and the hydrogen content in dry tail gas increases with the H 2 O:CH 4 ratio.*

35. Trimm, D. L. *Coke formation and minimisation during steam reforming reactions*. *Catalysis Today* vol. 37 (1997).

36. Chen, L., Qi, Z., Zhang, S., Su, J. & Somorjai, G. A. Catalytic hydrogen production from methane: A review on recent progress and prospect. *Catalysts* **10**, (2020).

37. Liu, C. J., Ye, J., Jiang, J. & Pan, Y. Progresses in the preparation of coke resistant Ni-based catalyst for steam and CO 2 reforming of methane. *ChemCatChem* vol. 3 529–541 (2011).

38. Hu, Y. H. & Ruckenstein, E. Catalytic Conversion of Methane to Synthesis Gas by Partial Oxidation and CO2 Reforming. *Advances in Catalysis* vol. 48 297–345 (2004).

39. Vogt, C. *et al.* Understanding carbon dioxide activation and carbon–carbon coupling over nickel. *Nature Communications* **10**, (2019).

40. Malerød-Fjeld, H. *et al.* Thermo-electrochemical production of compressed hydrogen from methane with near-zero energy loss. *Nature Energy* **2**, 923–931 (2017).

41. Kyriakou, V., Garagounis, I., Vourros, A., Vasileiou, E. & Stoukides, M. An Electrochemical Haber-Bosch Process. *Joule* **4**, 142–158 (2020).